COBEM 2023 27TH INTERNATIONAL CONGRESS OF MECHANICAL ENGENEERING

ABCM Brazilian Society of Mechanical Sciences and Engineering
27th ABCM International Congress of Mechanical Engineering
December 04-08, 2023, Florianópolis-SC, Brazil

COB-2023-1529
ANALYSIS OF THE MAGNETIC FIELD INFLUENCE ON FERROFLUID HEAT EXCHANGERS FOR APPLICATIONS IN THERMOACOUSTIC ENGINES

Arthur França Martins
Flávio de Campos Bannwart
Faculdade de Engenharia Mecânica - Universidade Estadual de Campinas/UNICAMP - Cidade Universitária Zeferino Vaz, Barão Geraldo, Campinas - SP, 13083-970
arthurfranca97@gmail.com
fcbannwart@fem.unicamp.br

Abstract. *Magnetic heat exchangers differ from conventional non-magnetic ones due to their susceptibility to a magnetic field, which can lead to a relevant heat flow if it is sufficiently intense. Such relevance, on the other hand, depends on the context of heat transfer demand, which guides the design of the heat exchanger. In this work, the fluids are a ferrofluid, which is a magnetic fluid that flows inside a copper tube, and atmospheric air as the external thermoacoustic working fluid. To correctly evaluate magnetic covection, it is necessary to have knowledge of several conditions such as applied magnetic field and its geometry, magnetic susceptibility of the ferrofluid, viscosity and conduction behavior as a function of the magnetic field. In this way, the study aims to understand the influence of the applied magnetic field on magnetic convection through the variation and evaluation of the magnetic Nusselt number via CFD in the context of a standing wave thermoacoustic engine application. In fact, results show that the way the magnetic field is applied produces a different induced magnetic field, which in turn directly influences the magnetic Nusselt number.*

Keywords: *heat exchanger, themomagnetic convection, thermoacoustics, ferrofluid, thermoacoustic engine*

1. INTRODUCTION

The growing demand for energy over the years (Ritchie *et al.*, 2022) combined with the need for increasingly cleaner and low-cost energy generation leads to new targeted research or methods that result in an increase in the efficiency of power cycles (namely the Rankine Cycle and the Brayton Cycle) or new possibilities for energy generation. However, the limited availability of sustainable heat sources is a significant challenge to the efficiency and viability of conventional power cycles. It is in this context that thermoacoustic engines appear, a promising alternative for power generation from low grade heat sources. These engines are based on principles of thermoviscous interaction between a gaseous fluid under resonant acoustic field and a solid substrate under sufficiently high temperature gradient, leading to the conversion of thermal energy into mechanical energy in its acoustic form (Hamood and Jaworski, 2023; Chen *et al.*, 2021). Unlike conventional cycles, thermoacoustic engines may work at relatively low thermal potential, depending on the heat source availability and its specific design features, *e.g.* static pressure, working gas, acoustic porous material and heat exchangers (Timmer *et al.*, 2018; Dong *et al.*, 2019), making them suitable to regenerate usually unavailable, such as industrial waste heat or low-temperature solar heat, the latter that may become an innovative and sustainable solution for power generation.

The standing wave thermoacoustic engine (TAE) essentially consists of heat exchangers (just one hot and one cold for the simplest configuration), one stack or acoustic porous material per thermoacoustic core, a resonator network and the working fluid (Swift, 1988). The stack is the most important component of the TAE, as within its porous the thermoacoustic phenomena takes place and the acoustic field is established. A good performing stack should minimize heat conduction along the temperature gradient direction and favor convective heat transfer within its pore internal walls; the resonator contains the stack and the heat exchangers, besides determining the fundamental resonant frequency, function of its length; the working fluid is a fundamental aspect to be considered in the TAE since the determination of the initial temperature difference, power and efficiency depend on its thermophysics properties; finally, the heat exchangers, where the hot heat exchanger supplies heat to the hot end of the stack and the cold heat exchanger extracts heat from the other end of the stack. Its characterization is crucial for a good TAE design and, to circumvent its difficult analytical modeling, has led to the development of specific experimental approaches (Bannwart *et al.*, 2012). Aiming at optimal operation, it is important that the heat exchanger has a high heat transfer coefficient and low acoustic power dissipation due to its acoustic impedance (Hariharan *et al.*, 2012; Swift, 1988).

Currently, there are several works that aim gains mainly in efficiency of heat exchangers. Among the various works there are Ajarostaghi *et al.* (2023), which employ a swirler device responsible for increasing the homogeneity of the flow; Marzouk *et al.* (2023), who use a fractal configuration in helical tubular heat exchangers, and mainly numerous works

such as Sahu *et al.* (2023), Hasan *et al.* (2023) and Ratul *et al.* (2023) that use alumina nanofluid (Al_2O_3) together with particles of other metals such as copper as a working fluid; Zhang *et al.* (2023) and Khedher *et al.* (2022) studied the influence of thermomagnetic convection on the heat exchanger.

The phenomenon of thermomagnetic convection occurs when there is a significant temperature gradient present in a magnetically susceptible fluid exposed to a sufficiently intense magnetic field. When such a fluid has the ability to become magnetized, then the fluid is said to be paramagnetic. The fluid of our case study, however, is called ferrofluid, as it consists of a stable colloidal dispersion of magnetic particles dispersed in a liquid carrier. The properties of ferrofluids are profoundly affected by the Brownian motion of the suspended particles and by the fact that each particle is permanently magnetized. In addition to the particles and the carrier liquid, the presence of a surfactant species is of fundamental importance in order to avoid the agglomeration of the particles among themselves (Rosensweig, 2014). As a first approach, the present work intends to analyze a heat exchanger of a thermoacoustic engine, with similar operation to the thermoacoustic refrigerator proposed by Bannwart and Arruda (2009), from the perspective of numerical simulation. To this end, fundamental concepts of heat exchangers will be validated through an analytical approach proposed by Ghosh *et al.* (2022) which will be extrapolated to other conditions analyzed.

2. THEORETICAL REFERENCE

As mentioned in the previous section, this study aims to address a heat exchanger in a thermoacoustic engine whose working fluid exhibits magnetic behavior. It is crucial to point out that, although they are similar terms, there is a clear distinction between ferrohydrodynamics (FHD) and magnetohydrodynamics (MHD). Ferrohydrodynamics concerns the area of fluid mechanics that investigates the movement of magnetic fluids under the influence of magnetic forces generated by field gradients. Magnetohydrodynamics, on the other hand, studies the behavior of electrically conductive fluids subject to a force, specifically the Lorentz Force per unit volume, resulting from an electric current (Rosensweig, 2014). Therefore, the focus of this work is the study of ferrohydrodynamics. As it deals with the coupling between various physics (energy, hydrodynamics and electromagnetism), it is necessary to present the expressions that govern each of these physics together with their considerations (boundary conditions).

2.1 Hydrodynamics

The first expression consists of the control volume mass balance expressed by Equation (1) for incompressible and steady-state flow.

$$\nabla \cdot \mathbf{V} = 0. \tag{1}$$

The Cauchy Equation for the ferrofluid is similar to the expression for a conventional fluid, differing in terms of the stress tensor. For this, the analysis is based on the equation of conservation of the internal angular momentum for a magnetic fluid, which can be written in the form of Equation (4) (Rosensweig, 2000).

$$\rho \frac{Ds}{Dt} = \rho G + \nabla \cdot C + A, \tag{2}$$

where s is the internal angular momentum per unit mass of the magnetic fluid caused by the rotation of the magnetic particles, G is the pair density of the magnetic body per unit mass, C is the tension tensor of the pair of surface and A is the vector anti-symmetric part of the viscous stress tensor representing the angular momentum conversion rate between external and internal forms. Expanding Equation (4) and performing the due simplifications and considerations, we obtain Equation (3) used in this work.

$$\rho_{eff} \frac{D\mathbf{V}}{Dt} = -\nabla p + (\eta_r + \zeta)\nabla^2 \mathbf{V} + 2\zeta(\nabla \times \boldsymbol{\omega}) + \mu_0(\mathbf{M} \cdot \nabla)\mathbf{H}, \tag{3}$$

with ρ_{eff} representing the effective specific gravity of the ferrofluid, $\mathbf{V}$ the velocity field, p the pressure field, η_r the viscosity ratio, ζ a vortex viscosity, $\boldsymbol{\omega}$ spin velocity, $\mathbf{M}$ the magnetization vector and $\mathbf{H}$ the applied magnetic field.

For comparative purposes, the Equation (4) consists of the Cauchy Equation with the Navier-Stokes tensor for any fluid. In general, it seems that the derivative terms of the material and the pressure gradient remain the same, while the diffusive term of Equation (3) presents a contribution from the viscosity of the vortex ζ and the body force term, which in Equation (4) represented only by $\mathbf{g}$ assumes the form relative to the magnetizing fields $\mathbf{M}$ and applied $\mathbf{H}$ as well as the contribution of rotational speed due to the tendency to align with the magnetic field.

$$\rho \frac{D\mathbf{V}}{Dt} = -\nabla p + \eta \nabla^2 \mathbf{V} + \rho \mathbf{g}. \tag{4}$$

Analogously, write the expression for angular momentum in the form of Equation (5) for magnetic particles.

$$\rho_p I \frac{D\boldsymbol{\omega}}{Dt} = \mu_0(\mathbf{M} + \mathbf{H}) + \eta' \nabla^2 \boldsymbol{\omega} + 2\zeta(\nabla \times \mathbf{V} - 2\boldsymbol{\omega}), \tag{5}$$

where ρ_p represents the specific mass of the particle, I the moment of inertia of the particle, η' spin viscosity and μ_0 the magnetic permeability of vacuum.

2.2 Magnetism

The Magnetization vector M is given by the product between the magnetic susceptibility χ and the magnetic field H (Rosensweig, 2014). Magnetic susceptibility, in turn, measures the ability of a material to become magnetized under the action of magnetic stimulation from a magnetizing field to which it is subjected. The response to the stimulus is expressed in the form of a M magnetization of the material, and there are materials that respond in a way that weakly opposes the presence of the stimulus inside and there are those that respond weakly in favor of the stimulus, both doing so. not generally proportional to the stimulus. The former are classified as diamagnetic materials and the latter constitute the group of paramagnetic materials (Griffiths, 2017). In this way, the expression for the magnetization of the particle is given by Equation (6) (Rosensweig, 2000).

$$\frac{D\mathbf{M}}{Dt} = \boldsymbol{\omega} \times \mathbf{M} - \frac{1}{\tau}(\mathbf{M} - \mathbf{M}_0). \tag{6}$$

For the formulation of the interaction of the magnetic field, a set of four Equations is used: Gauss' Law given by Equation (7); Gauss's Law for Magnetism given by Equation (8); Faraday's Law of Induction given by Equation (9) and Ampère-Maxwell's Law given by Equation (10).

$$\nabla \cdot \mathbf{E} = \frac{\rho_c}{\varepsilon_0}, \tag{7}$$

$$\nabla \cdot \mathbf{B} = 0, \tag{8}$$

$$\nabla \times \mathbf{E} = -\frac{\partial \mathbf{B}}{\partial t}, \tag{9}$$

$$\nabla \times \mathbf{B} = \mu_0 \mathbf{J} + \mu_0 \varepsilon_0 \frac{\partial \mathbf{E}}{\partial t}, \tag{10}$$

where ρ_c represents the charge density of the medium, ε_0 the electrical permittivity of the medium and $\mathbf{J}$ the current density.

Considering that the induced Magnetic Field $\mathbf{B}$ is given by $\mathbf{B} = \mu_r \mathbf{H}$ with μ_r being the relative permeability of the medium, it is possible to rewrite Equation (10) in terms of the applied magnetic field $\mathbf{H}$, that is, Equation (11), which is more interesting from the point of view of ferrohydrodynamics.

$$\nabla \times \mathbf{H} = \mathbf{J} + \varepsilon_0 \frac{\partial \mathbf{E}}{\partial t}. \tag{11}$$

For the FHD context, Equations (7), (8), (9) and (11) known as the Maxwell's Equations now consider the limit magnetostatic, that is, the effects of electric current flow and electric field are considered negligible so that $\mathbf{J} = 0$, $\mathbf{E} = 0$ and $\partial \mathbf{B} \,/\partial t = \mathbf{0}$, which implies $\nabla \times \mathbf{H} = \mathbf{0}$.

2.3 Energy

Finally, consider the expression for energy in the form of heat given by Equation (12).

$$\rho_{eff} c_p \frac{DT}{Dt} = \nabla \cdot (K_{eff} \nabla T) + q''' + \eta_{eff} \Phi, \tag{12}$$

With c_p corresponding to the specific heat at constant pressure, K_{eff} the effective thermal conductivity, q''' volumetric rate of heat regeneration and Φ the viscous dissipation.

2.4 Validation

To perform the following analyses, the parameters of the governing equations (hydrodynamics, magnetism and energy) are dimensionless as follows:

$$x^* = \frac{x}{h}, y^* = \frac{y}{h}, p^* = \frac{p}{\rho U^2}, H_y^* = \frac{H_y}{H_0}, T^* = k\frac{T - T_1}{q_1 h}$$

.

Equation (13) was obtained by Ghosh *et al.* (2022) starting from equations similar to those mentioned in previous subsections with considerations also implemented by this work.

$$Nu_c = K\left\{-q\left(\frac{3D^2}{280} - \frac{3D}{20} + \frac{2}{5}\right) + \frac{1}{\eta_r}\left[\frac{BrD^4}{2240} - \frac{BrD^3}{70} + D^2\left(\frac{39Br}{280} + \frac{13\eta_r}{420}\right) - D\left(\frac{2Br}{5} + \frac{13\eta_r}{30}\right) + \frac{7Br}{20} + \frac{8\eta_r}{5}\right]\right\}^{-1} \quad (13)$$

where q corresponds to the heat rate, Br corresponds to the Brinkman number, η_r the viscosity ratio, K as defined to $K = (D-6)^2/6$ and D is obtained through Equation (14) as:

$$D = Re_d \eta_r \frac{dp^*}{dx^*}\left[1 + \frac{3}{2}\varphi\eta_r(1-z)\right]^{-1}, \quad (14)$$

with Re_d representing the Reynolds number, $dp*/dx*$ the dimensionless pressure gradient in the x direction, φ being the volumetric fraction of the magnetic particles and z obtained by solving Equation (15)

$$z = \frac{4}{4 + M_{nf} L(H_y^*)\tau^* H_y^{*2}}, \quad (15)$$

where M_{nf} corresponds to the magnetic flux number, $L(H_y^*)$ the dimensionless Langevin function given by $L(H_y^*) = coth(\lambda_0 H_y^*) - (\lambda_0 H_y^*)^{-1}$. Proofs and more details are available in Ghosh *et al.* (2022)'s work.

Table 1. Properties of the ferrofluid used in the simulation.

Quantity	**Value**$^{(1)}$
Specific mass	1210 $^{kg}/_{m^3}$
Dinamic viscosity	6 $^{mPa}/_{s}$
Thermal conductivity	0.19 $^{W}/_{m \cdot K}$
Heat capacity	1840 $^{J}/_{kg \cdot K}$
Thermal expansion coefficient	8.6·10^{-4} $^{1}/_{K}$
Saturation magnetization	44 mT
Initial Magnetic Susceptibility	2.64

$^{(1)}$ Regarding the EFH1 ferrofluid type.

3. METHODOLOGY

As explained above, the present work will analyze the heat exchanger of a thermoacoustic engine through parametric variation and comparison with analytical solutions when possible. Figure 1 presents the 3D schematic model of the heat exchanger. This model is composed of a waveguide (larger cylinder) and a parallelepiped that crosses it perpendicularly. Although there is an indication of inlet and outlet flow in the waveguide by Figure 1, it is known that there is no net flow inside the thermoacoustic engine, but oscillation of the acoustic particles around a midpoint . On the other hand, the parallelepiped that crosses the waveguide is responsible for conducting the ferrofluid inside and therefore will be the main target of analysis. Aiming at validating the numerical model by means of empirical expressions, the flow of the duct with a rectangular section that conducts the fluid iron was first treated as a flow between flat plates of the type shown in Figure 2 and, later modifications will be made in the numerical model in order to determine optimal values that maximize the heat extraction by the ferrofluid. For the sake of ease of explanation, the methodology will be divided between the three physics: hydrodynamics, magnetism and energy (heat).

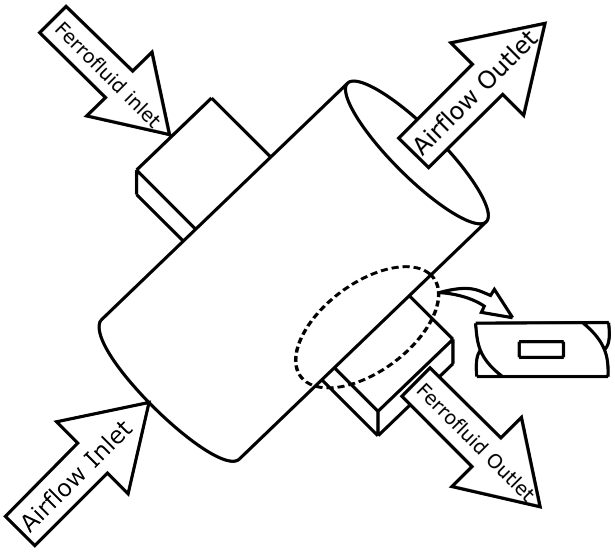

Figure 1. Schematic Model of the thermoacoustic engine heat exchanger.

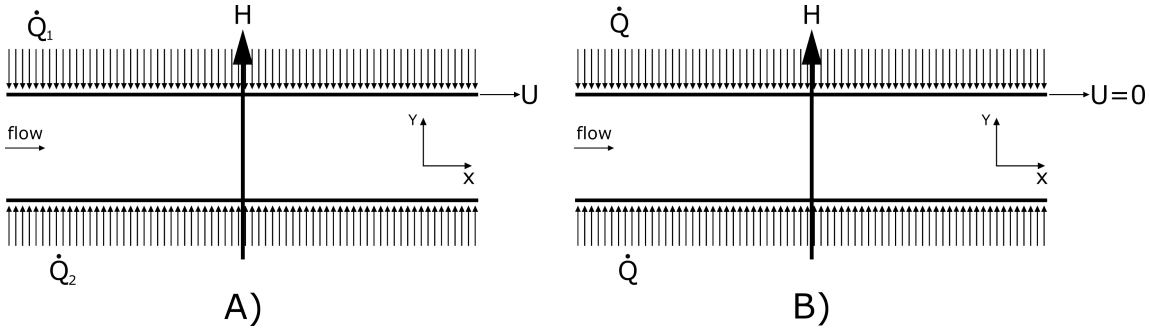

Figure 2. Studied models. A) Ghosh *et al.* (2022) e B) this work.

3.1 Hydrodynamics

The Figure 3 has two main elements seen from above and sideways, the first one consists of a parallelepiped in ( ) color, which implements the domain technique infinite so that it acts as two flat plates, where the ferrofluid flow occurs. On the side there are two cylinders in ( ) color, which will be addressed in the topic on magnetism, which represent two electromagnets. Regarding the boundary conditions, a fluid is defined with the properties present in Table 1 with input located on the left part of Figure 3 and output on the right , being input with 5 cm/s and output with zero pressure difference. Furthermore there is gravity oriented in the negative direction of *Z*.

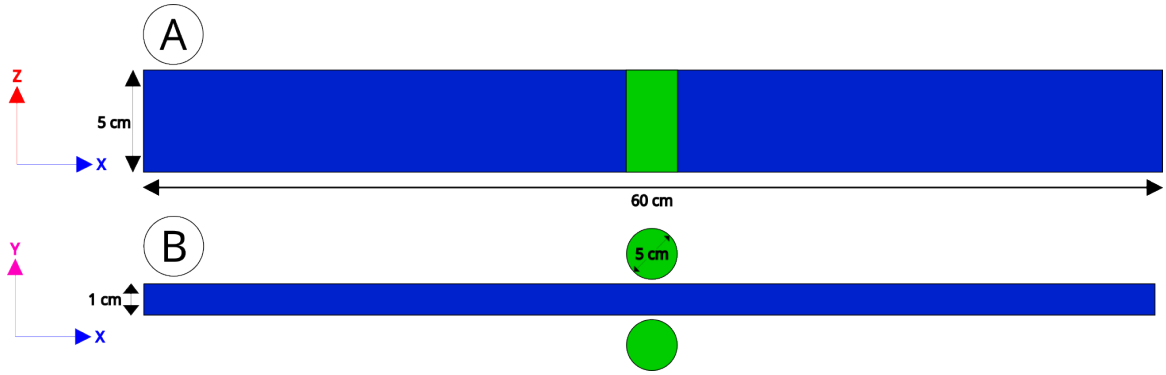

Figure 3. Numeric Fluid and Energy Domain.

3.2 Magnetism

Figure 4 is an extension of Figure 3, i.e., an air envelope in the heat exchanger, in ( ) color, whose function is to be a magnetic insulator. As for the boundary conditions, the cylinder mentioned in the previous section corresponds to

an electromagnet so that the cylinder acts as a solenoid with an iron core (since the cylinder material is specified as iron), so that each solenoid is excited by a current of 1A and the direction of the Magnetic Force (right-hand rule) pointed in the positive Z direction. Furthermore, each solenoid has a winding of 100 turns. The parallelepiped where the fluid iron flow occurs is said to be a perfect magnetic conductor and defined as a new domain for applying Ampere's Law Equation (10) so that as input it receives a magnetization curve $B \times H$ characteristic of the ferrofluid already specified in this work. Finally, the larger parallelepiped is defined as insulating and material being air.

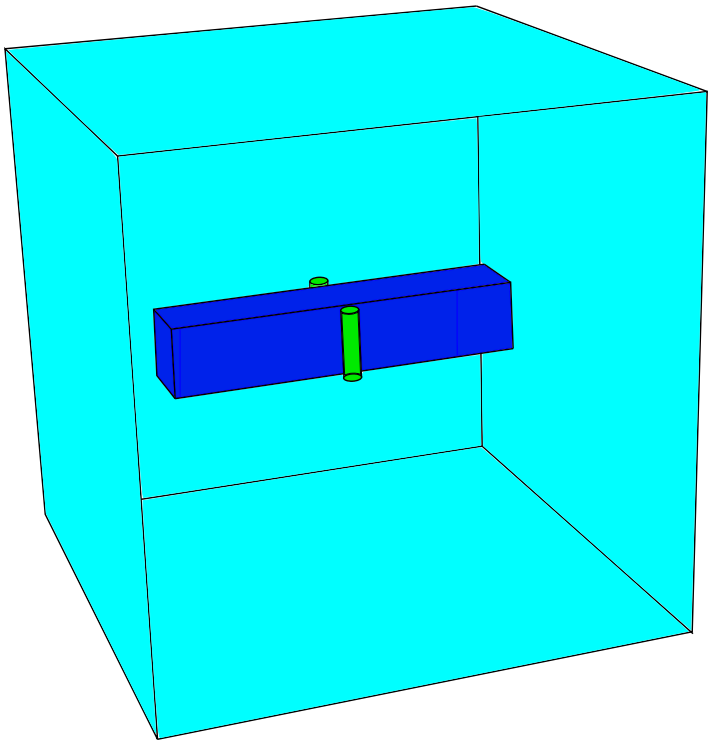

Figure 4. Full Numeric Domain.

3.3 Energy

The energy model is defined in the same domain as Figure 3. For this, the same inlet and outlet of the fluid already specified in the Hydrodynamics section is defined for a for a correct coupling between the physics of hydrodynamics and the plate temperature as being constant at 800 K.

3.4 Additional Settings

For a correct coupling of physics in COMSOL, it is necessary to insert additional parameters such as viscosity and thermal conduction, that is, physically the magnetic field alters the physical properties of the fluid depending on the orientation in which this field is applied. Due to the current configuration of the numerical model, which employs a magnetic field perpendicular to the flow of the ferrofluid, thus resulting in a greater viscosity of the same as a function of the field and, although the field does not vary in time, it varies in space, so the fluid perceives a variation in its viscosity in space. The same is true for thermal conduction. Therefore, aiming at a better representation of the physics involved, the Equations (16) and (18) were inserted in COMSOL and assigned to the materials involved in the model.

$$k_{\perp} = k_0 \frac{(1-\varphi_{int})^{-3} + \frac{\varphi}{\varphi_{int}}[(1-\varphi_{int})^{-3} - 1] + 1}{(1-\varphi_{int})^{-3} - \frac{\varphi}{\varphi_{int}}[(1-\varphi_{int})^{-3} - 1] + 1}, \tag{16}$$

where k_0 corresponds to the thermal conductivity of the ferrofluid and φ_{int} obtained by solving Equation (17).

$$\varphi_{int} = (\varphi_m - \varphi_h) tanh\left[c(\gamma H \varphi \varphi_h)^2\right] + \varphi_h, \tag{17}$$

Being φ_{int} the volume fraction of nanoparticles in aggregates, φ_m the maximum volume fraction, φ_h hydraulic volume fraction, c the compression parameter and γ defined as a ratio of the initial magnetic susceptibility χ_0 to the magnetic saturation M_s, that is $\gamma = 3\chi_0/M_s$.

$$\eta_{eff} = \eta_0 \left(1 + \frac{3}{2}\frac{\gamma H - tanh(\gamma H)}{\gamma H + tanh(\gamma H)}\right), \tag{18}$$

4. RESULTS

Solving the Equation (13), we obtain as a result the Figure 5 representing the behavior in the Nusselt number for the model already described as a function of the applied magnetic field. It is verified that the Nusselt number increases as the magnetic field increases, a behavior that is in line with other works such as Ashouri *et al.* (2010) and Bahiraei and Hangi (2013).

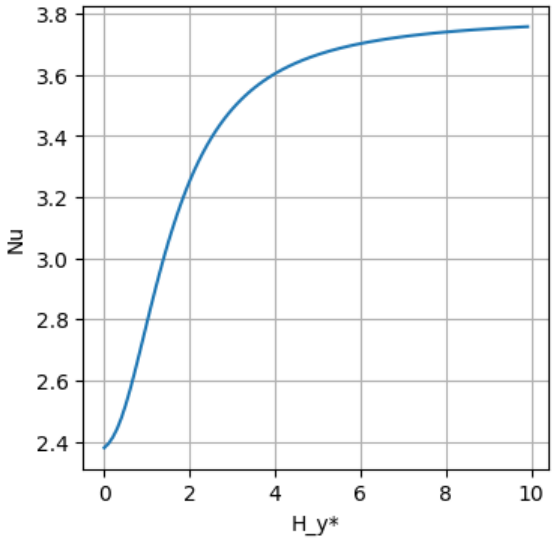

Figure 5. Nusselt number as magnetic field function.

As described in previous sections, the simulation was performed translating into Figure 6. Note that in the region close to the coil (region circled in black) there is a difference in the temperature pattern of the ferrofluid, so that the layers of higher temperature (zones in red to yellow) are smaller in size. In addition, there is no predominance of strong blue zones in the location, unlike other regions, indicating that there is greater homogeneity in the region. Such a change in the temperature profile is due to the magnetic field inside, given that such change persists only around the coil.

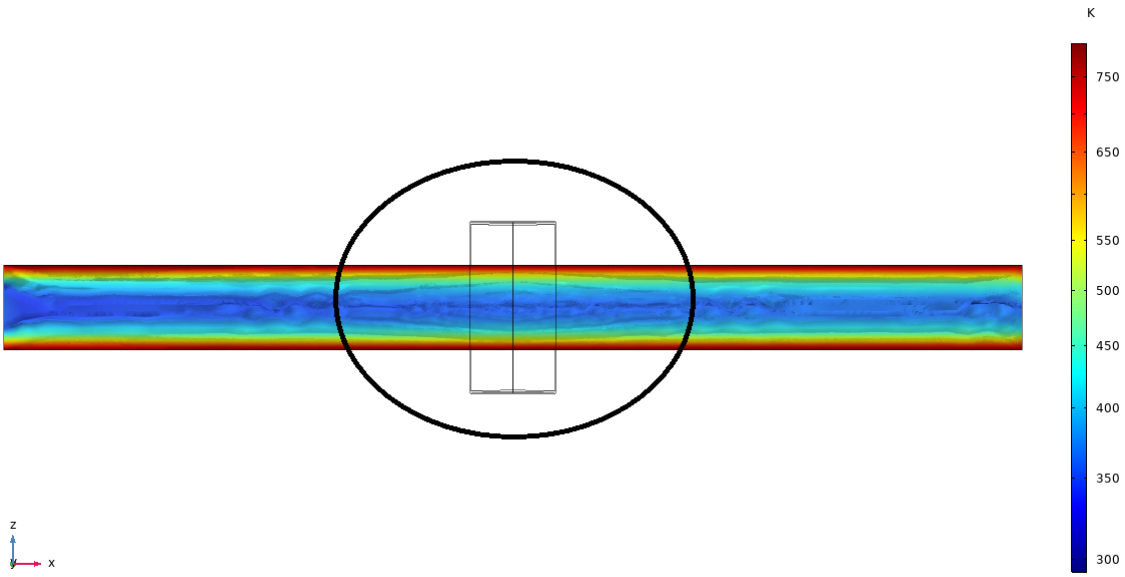

Figure 6. Temperature profile for ferrofluid flow.

Finally, when calculating the Nusselt Number along the length of the heat exchanger, Figure 7 is obtained, so that the average Nusselt Number along the flow is 3.003, This value is close to the analytical one for $H_y^* = 1$ whose value is 2.784.

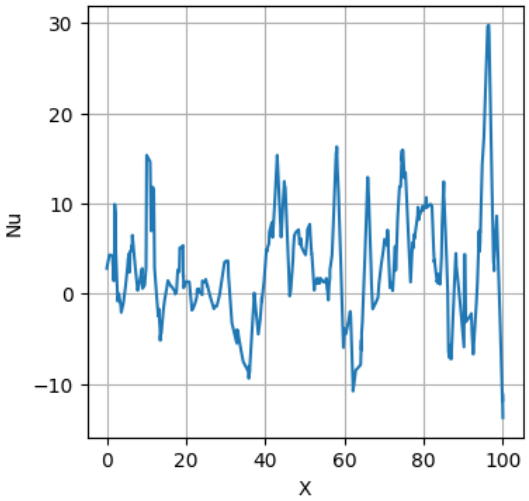

Figure 7. Nusselt number as length function of heat exchanger.

After validating the numerical model through analytical expressions, two operational configurations related to the magnetic field were changed, first being the position of the coils (or electromagnet) and the second consisting of increasing the number of coils. Figure 8 shows the change in the position of the coils, in which it is initially seen that there is an extension of the fluid disturbance zone demonstrated by the black circles. This phenomenon occurs because the electromagnets positioned above and below (configuration B) of the exchanger direct the magnetic flux into the exchanger, while positioning the coils laterally only diverts part of the magnetic flux (configuration A). The Figures that show the profile of the induced magnetic field (B) present higher values for configuration B, reaching 1.2 T in the coil and 0.76 T in the fluid while configuration A presents 1 T in the coil and 0.33 T in the fluid. Therefore, directing the magnetic field lines towards the ferrofluid results in a greater induced field, given that the presence of a magnetic field H magnetizes the iron particles in the suspension, which in turn act as small magnets, thus contributing to a larger induced field and, in turn, this larger induced field results in a larger Nusselt number, in this case, 3.003 for configuration A and 3.815 for configuration B.

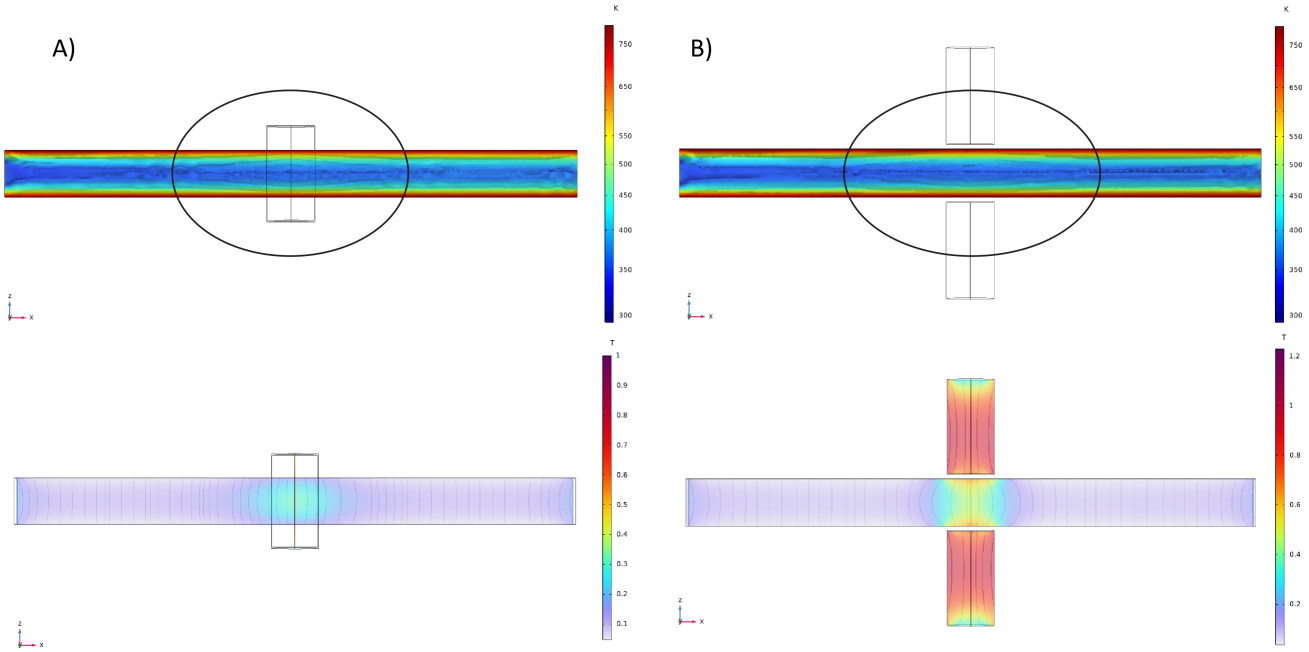

Figure 8. Comparison between coil configurations.

Figure 9 in turn presents a greater number of inductors, all made of the same material, same current and same number of turns. Comparing configurations A and B, it was found that there was also an extension of the fluid disturbance zone, as each pair of coils generates the same field, so such behavior was in fact expected. However, when comparing the induced magnetic fields, it was noticed that there is a small increase in the induced magnetic field as it passes through the coils. It is believed that this behavior occurs because the ferrofluid passes through the coils in a time shorter than the relaxation time. magnetic so that it arrives at the subsequent coil still magnetized, contributing incrementally to each coil. Finally, the Nusselt number was found to be 3.003 for configuration A and 3.301 for configuration B.

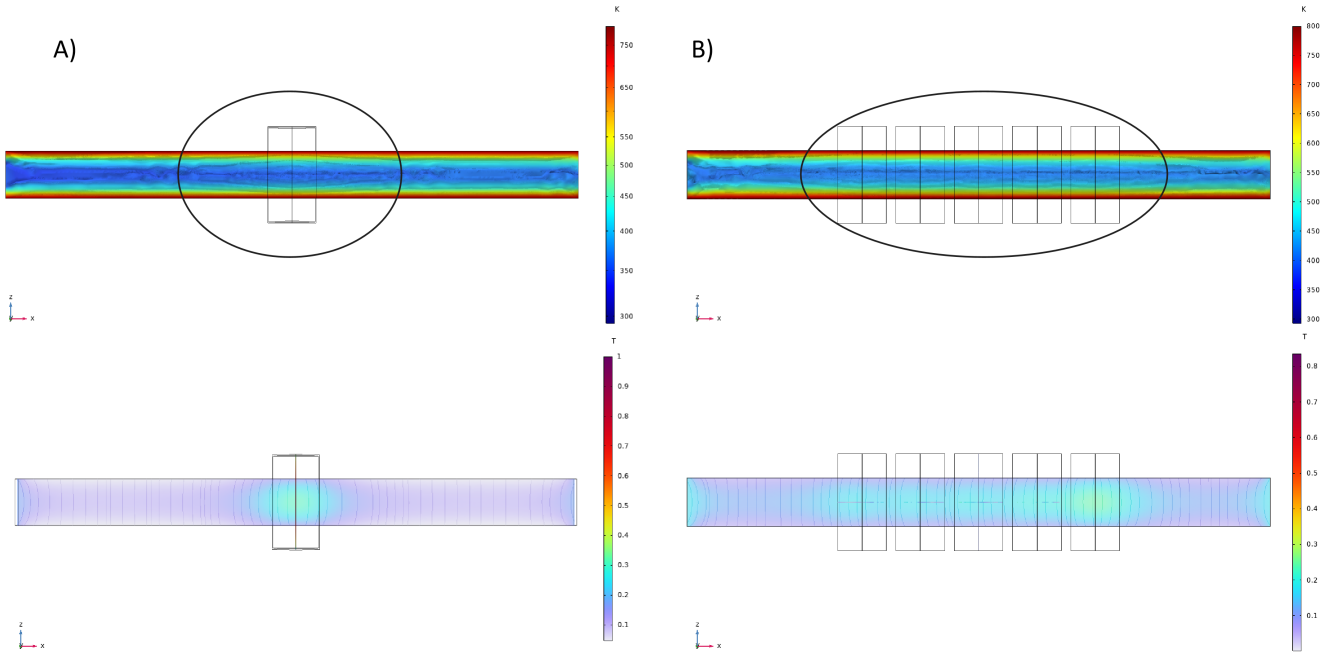

Figure 9. Comparison between number of coils.

5. CONCLUSIONS

The results show the location of the coils directly affected by the induced magnetic field modulus even though the magnetic field applied is constant in time and direction at each evaluation. As a result of the increase in the magnetic field induced either by the orientation of the coils or its quantity, it is observed that the increase in the intensity of the induced field causes an increase in the Nusselt number up to the point of magnetic saturation. Furthermore, it should be noted that adding coils locally increases the induced field due to the ferrofluid's magnetization. Therefore, it is conveyed that the presence of the magnetic field leads to an increase in the Nusselt number.

6. ACKNOWLEDGEMENTS

We thank the Faculty of Mechanical Engineering (FEM) of University of Campinas (UNICAMP) for providing the structure and equipment to carry out this study. This work was has been funded by Foundation for Research and Scientific and Technological Development of Maranhão (FAPEMA) under project number BM-01657/23.

7. REFERENCES

Ajarostaghi, S.S.M., Karouei, S.H.H., Alinia-kolaei, M., Karimi, A.A., Zadeh, M.M. and Sedighi, K., 2023. "On the Hydrothermal Behavior of Fluid Flow and Heat Transfer in a Helical Double-Tube Heat Exchanger with Curved Swirl Generator; Impacts of Length and Position". *Energies*, Vol. 16, No. 4, p. 1801. doi: https://doi.org/10.3390/en16041801.

Ashouri, M., Ebrahimi, B., Shafii, M., Saidi, M. and Saidi, M., 2010. "Correlation for nusselt number in pure magnetic convection ferrofluid flow in a square cavity by a numerical investigation". *Journal of Magnetism and Magnetic Materials*, Vol. 322, No. 22, pp. 3607–3613. doi:https://doi.org/10.1016/j.jmmm.2010.05.041.

Bahiraei, M. and Hangi, M., 2013. "Investigating the efficacy of magnetic nanofluid as a coolant in double-pipe heat exchanger in the presence of magnetic field". *Energy Conversion and Management*, Vol. 76, pp. 1125–1133. ISSN 0196-8904. doi:https://doi.org/10.1016/j.enconman.2013.09.008.

Bannwart, F. and Arruda, J., 2009. "Construction of a demonstrative apparatus for the thermoacoustic refrigeration effect".

Bannwart, F., Penelet, G., Lotton, P. and Dalmolt, J.P., 2012. "Methods for transfer matrix evaluation applied to thermoacoustics".

Chen, G., Tang, L., Mace, B. and Yu, Z., 2021. "Multi-physics coupling in thermoacoustic devices: A review". *Renewable and Sustainable Energy Reviews*, Vol. 146, p. 111170. doi:https://doi.org/10.1016/j.rser.2021.111170.

Dong, S., Shen, G., Xu, M., Zhang, S. and An, L., 2019. "The effect of working fluid on the performance of a large-scale thermoacoustic stirling engine". *Energy*, Vol. 181, pp. 378–386. doi:https://doi.org/10.1016/j.energy.2019.05.142.

Ghosh, D., Meena, P.R. and Das, P.K., 2022. "A fully analytical solution of convection in ferrofluids during Couette-Poiseuille flow subjected to an orthogonal magnetic field". *International Communications in Heat and Mass Transfer*, Vol. 130, p. 105793. doi:https://doi.org/10.1016/j.icheatmasstransfer.2021.105793.

Griffiths, D.J., 2017. *Introduction to Electrodynamics*. Cambridge University Press, 4th edition. doi:10.1017/9781108333511.

Hamood, A. and Jaworski, A.J., 2023. "Thermoacoustic cascade engine free from resonance length". *Energy*, Vol. 271, p. 126881. doi:https://doi.org/10.1016/j.energy.2023.126881.

Hariharan, N., Sivashanmugam, P. and Kasthurirengan, S., 2012. "Influence of stack geometry and resonator length on the performance of thermoacoustic engine". *Applied Acoustics*, Vol. 73, No. 10, pp. 1052–1058. doi:https://doi.org/10.1016/j.apacoust.2012.05.003.

Hasan, M.F., Danışmaz, M. and Majel, B.M., 2023. "Thermal performance investigation of double pipe heat exchanger embedded with extended surfaces using nanofluid technique as enhancement". *Case Studies in Thermal Engineering*, Vol. 43, p. 102774. doi:https://doi.org/10.1016/j.csite.2023.102774.

Khedher, N.B., Shahabadi, M., Alghawli, A.S., Hulme, C.N. and Mehryan, S.A.M., 2022. "Numerical Study of the Flow and Thermomagnetic Convection Heat Transfer of a Power Law Non-Newtonian Ferrofluid within a Circular Cavity with a Permanent Magnet". *Mathematics*, Vol. 10, No. 15, p. 2612. doi:https://doi.org/10.3390/math10152612.

Marzouk, S., Abou Al-Sood, M., El-Said, E.M., Younes, M. and El-Fakharany, M.K., 2023. "Experimental and numerical investigation of a novel fractal tube configuration in helically tube heat exchanger". *International Journal of Thermal Sciences*, Vol. 187, p. 108175. doi:https://doi.org/10.1016/j.ijthermalsci.2023.108175.

Ratul, R.E., Ahmed, F., Alam, S., Rezwanul Karim, M. and Bhuiyan, A.A., 2023. "Numerical study of turbulent flow and heat transfer in a novel design of serpentine channel coupled with D-shaped jaggedness using hybrid nanofluid". *Alexandria Engineering Journal*, Vol. 68, pp. 647–663. doi:https://doi.org/10.1016/j.aej.2023.01.061.

Ritchie, H., Roser, M. and Rosado, P., 2022. "Energy". *Our World in Data*. Https://ourworldindata.org/energy.

Rosensweig, R.E., 2000. "Role of internal rotationsin selected magnetic fluid applications". *Magnetohydrodynamics*, Vol. 36, No. 4, pp. 241–253. doi:10.1023/A:1010470504723. URL `http://www.kluweronline.com/article.asp?PIPS=345321`.

Rosensweig, R., 2014. *Ferrohydrodynamics*. Dover Publications, 1st edition.

Sahu, M., Sarkar, J. and Chandra, L., 2023. "Experimental thermal-hydraulic characteristics of single-phase natural circulation loop using water-based hybrid nanofluids". *International Journal of Thermal Sciences*, Vol. 187, p. 108198. doi:https://doi.org/10.1016/j.ijthermalsci.2023.108198.

Swift, G.W., 1988. "Thermoacoustic engines". *The Journal of the Acoustical Society of America*, Vol. 84, No. 4, pp. 1145–1180. doi:https://doi.org/10.1121/1.396617.

Timmer, M.A.G., De Blok, K. and Van Der Meer, T.H., 2018. "Review on the conversion of thermoacoustic power into electricity". *The Journal of the Acoustical Society of America*, Vol. 143, No. 2, pp. 841–857. doi:https://doi.org/10.1121/1.5023395.

Zhang, W., Li, G.J., Ren, B., Chong, Y.C. and Michon, M., 2023. "Investigation of Ferrofluid Cooling for High Power Density Permanent Magnet Machines". *IEEE Transactions on Magnetics*, Vol. 59, No. 1, pp. 1–11. doi:https://doi.org/10.1109/TMAG.2022.3224787.

8. RESPONSIBILITY NOTICE

The authors are solely responsible for the printed material included in this paper.